ELSEVIER

Journal of Crystal Growth 235 (2002) 603–618

JOURNAL OF CRYSTAL GROWTH

www.elsevier.com/locate/jcrysgro

Simulation of crystal shape evolution in two dimensions

E. van Veenendaal[a,*], A.J. Nijdam[b], J. van Suchtelen[a,b]

[a] RIM Department of Solid State Chemistry, Faculty of Science, University of Nijmegen, Toernooiveld, 6525 ED Nijmegen, The Netherlands

[b] MESA+ Research Institute, University of Twente, P.O. Box 217, 7500 AE Enschede, The Netherlands

Received 12 February 2001; accepted 18 October 2001

Communicated by J.J. Derby

Abstract

We present a simulation tool for the prediction of the evolution of macroscopic crystal growth and etching shapes that can be represented in a two-dimensional setting. It is assumed that the advance rate of the crystal surface depends solely on the surface orientation, which implies that the classical kinematic wave theory applies. We present an algorithm to calculate the crystal shape at any given point in time in a single time step for initial crystal shapes that are either completely convex or completely concave. We show that calculation of the crystal shape for mixed convex/concave crystal shapes may require a series of time steps. Boundary conditions imposed at imperfections in the crystal surface or at boundaries with a container wall or a mask are treated. The possibility of two or more disconnected crystal shapes that meet at some point in their evolution is also taken into account. The simulation tool is used to predict crystal shape evolution for the technologically relevant case of wet chemical etching of masked silicon {1 0 0} wafers with multiple mask openings. It is shown that the experimental evolution of Si{1 1 0} surfaces cannot be reproduced using any simulation tool based on the assumption that the etch rate depends solely on the surface orientation. The differences between experiments and simulations are explained on the basis of the etching mechanism of Si{1 1 0} surfaces. © 2002 Elsevier Science B.V. All rights reserved.

PACS: 68.10.Jy; 82.20.Wt

Keywords: A1. Computer simulation; A1. Interfaces

1. Introduction

Crystal growth and etching have been investigated extensively using atomistic models, which has resulted in valuable insight in the growth and etching mechanisms of crystal surfaces with near-facet orientations [1–3]. However, for the purpose of predicting the evolution of macroscopic crystal growth and etching shapes, it seems more appropriate to use a continuum description, where the crystal surface is regarded as a sharp mathematical surface. Each point on such a surface can be designated its own growth or etch rate perpendicular to the surface. In general, this advance rate depends on the local surface orientation and the local driving force for crystallization or

*Corresponding author. Tel.: +31-24-3653326; fax: +31-24-3553450.

E-mail address: erikvv@sci.kun.nl (E. van Veenendaal).

0022-0248/02/$ - see front matter © 2002 Elsevier Science B.V. All rights reserved.
PII: S0022-0248(01)01832-2

dissolution. The local driving force is determined by the local composition and temperature of the solution and also by the local curvature of the surface, which give rise to the Gibbs–Thomson shift [4]. Here, we assume that solute diffusion in the solution and diffusion of heat are very fast, which implies that growth or etching is purely geometric, i.e., the growth or etch rate depends only on the local shape of the crystal. Geometric models of crystal growth have been studied extensively, for a review, see Ref. [5]. In this paper, we also assume that curvature effects may be neglected, which implies that the driving force is homogeneous over the crystal surface. Effectively, this means that we restrict ourselves to the case where the orientation of the surface is the only parameter in the growth or etch rate function. This specific case of interface motion is described by the classical kinematic wave theory, which is developed for crystal growth and etching by Frank [6] and Chernov [7].

In this paper, we present a simulation tool for the prediction of the evolution of macroscopic crystal growth and etching shapes that can be described in a two-dimensional setting. First of all, the tool can predict the evolution of step patterns on a crystal facet. Secondly, it can be used to predict the evolution of (parts of) three-dimensional crystals that can be fully described by a two-dimensional cross-section. Essential for the applicability of the simulation tool is detailed knowledge of the growth or etch rate of the crystal at the experimental conditions under consideration. In a previous paper, we have described a construction method for analytical orientation dependent growth and etch rate functions containing only a small number of, physically meaningful, parameters [8,9]. These functions are very useful in continuum simulations of crystal growth or etching.

The paper is structured as follows. In Section 2, we present a survey of the classical kinematic wave theory in two dimensions. Next, in Section 3, we present the simulation algorithms. We emphasize the complications that may arise when the initial crystal shape consists of both convex and concave parts. For an initial shape that is completely convex or completely concave the final crystal shape can be calculated in a single step, while for a mixed convex/concave initial shape several calculation steps may be required. The simulation tool can take into account local imperfections of the crystal surface and it can deal with two or more disconnected crystal shapes that meet at some point in time. In Section 4, we elaborate on a technologically relevant example that highlights all features of the simulation tool: wet chemical etching of masked silicon $\{1\,0\,0\}$ wafers with multiple mask openings. Finally, in Section 5 we discuss the difficulties that will be encountered when extending the algorithms to three dimensions.

2. The kinematic wave theory

The classical kinematic wave theory developed by Frank and Chernov [6,7] is the continuum description of crystal growth and etching for the case that the growth or etch rate $R(\boldsymbol{n})$ or $R(\phi)$ is uniquely determined by the normal orientation of the surface, $\boldsymbol{n} = (\cos\phi, \sin\phi)$. Originally, this is hardly a theory on crystal growth, but rather a description of interfaces propagating with an orientation dependent rate: it is a generalization of Huygens' principle for propagating wave fronts [10].

In this paper, we adhere to the convention that the two-dimensional normal vector $\boldsymbol{n}$ points in the direction of propagation, i.e. from crystal to parent phase for growth, in the opposite direction for etching. It is convenient to define the polar-plotting vector operator $\mathbf{P}$, the "Gibbs–Wulff" vector operator $\mathbf{Q}$ and the stiffness tensor operator $\mathbf{S}$ operating on the propagation rate $R(\phi)$,

$$\mathbf{P}R(\phi) = R(\phi)(\cos\phi, \sin\phi), \tag{1}$$

$$\mathbf{Q}R(\phi) = R(\phi)(\cos\phi, \sin\phi) + \frac{\mathrm{d}R(\phi)}{\mathrm{d}\phi}(-\sin\phi, \cos\phi), \tag{2}$$

$$\mathbf{S}R(\phi) = R(\phi) + \frac{\mathrm{d}^2R(\phi)}{\mathrm{d}\phi^2}. \tag{3}$$

When the advance rate depends solely on the orientation, loci of constant orientation follow straight lines: the kinematic wave trajectories as

Frank called them [6]. By definition the advance rate of the surface is constant following these trajectories, hence we can define the vector velocity of the surface along such a trajectory. This vector velocity equals the vector $\mathbf{Q}R(\phi)$ [11]. In the papers of Cahn and coworkers, this description of the motion of the interface is called the gradient formulation [5,12]. The vector $\mathbf{Q}R(\boldsymbol{n})$ equals the characteristic of motion $\chi(\boldsymbol{n}) = \nabla R_e(\boldsymbol{p})$, where $R_e(\boldsymbol{p})$ is the extension of $R(\boldsymbol{n})$ to all vectors: $R_e(\boldsymbol{p}) = \|\boldsymbol{p}\| R(\boldsymbol{p}/\|\boldsymbol{p}\|)$. Another useful quantity is the rate of change of the inverse of the surface curvature following the surface along a kinematic wave trajectory. It can be shown that this rate of change equals the inverse of the second fundamental tensor of the $\mathbf{Q}R(\boldsymbol{n})$ surface, which we call $\mathbf{S}R(\boldsymbol{n})$ [11]. For interface motion in two dimensions $\mathbf{S}R(\boldsymbol{n})$ equals the one-dimensional tensor defined in Eq. (3).

Now we will introduce the analytical advance rate $R(\phi)$ that we will use for all illustrations in this and the next section. This choice for the advance rate function is

$$\begin{aligned} R(\phi) = \lceil -4 \rfloor & v_{10} \lceil 2 \rfloor \sin(\phi)\, \varepsilon_{10} \lfloor\, \rceil, \\ & v_{10} \lceil 2 \rfloor \sin\left(\phi + \frac{\pi}{2}\right) \varepsilon_{10} \lfloor\, \rceil, \\ & v_{11} \lceil 2 \rfloor \sin\left(\phi - \frac{\pi}{4}\right) \varepsilon_{11} \lfloor\, \rceil, \\ & v_{11} \lceil 2 \rfloor \sin\left(\phi + \frac{\pi}{4}\right) \varepsilon_{11} \lfloor\, \rceil \lfloor\, \rceil, \end{aligned} \tag{4}$$

where $\lceil a \rfloor \; F, G, H, \ldots \; \lfloor\, \rceil \equiv [F^a + G^a + H^a + \cdots]^{1/a}$. The use of this mathematical operation, which we call assembling operation, is further explained in Ref. [8]. This function describes growth or etching of a square crystal with two facet orientations, $\{1\,0\}$ and $\{1\,1\}$. The advance rate function contains four physically meaningful parameters: two parameters for each family of facets. The function assembles the complete advance rate function from the advance rates in the vicinity of the facet orientations. The four operands of the outer assembling operation describe the growth or etch rate in the vicinity of a facet orientation. The advance rate of a vicinal facet is supposed to stem from the competition of two processes: misorientation step flow and nucleation of monolayer islands or pits. The parameters v_{10} and v_{11} are the step velocities on the $\{1\,0\}$ and $\{1\,1\}$ facets, respectively. The parameters ε_{10} and ε_{11} describe the relative importance of nucleation and step flow for the $\{1\,0\}$ and $\{1\,1\}$ facets, respectively. ε equal to 0 represents the case that nucleation can be neglected. The parameter ε can be related to ΔG^*, the free energy needed to form a critical nucleus on the facet, and as such can be viewed as a measure of the surface roughness [8].

We have chosen to consider the case $v_{10} = v_{11}$ and $\varepsilon_{10} = 0.15$, $\varepsilon_{11} = 0.25$. In Fig. 1 the polar plot for the advance rate, $\mathbf{P}R(\phi)$, is drawn. Also depicted is the $\mathbf{Q}R$-shape, which displays many self-intersections, forming "ears". Notice that each minimum of $R(\phi)$ corresponds to a convex section of the $\mathbf{Q}R$-shape, and that, for this example, each maximum of $R(\phi)$ corresponds to a concave section of the $\mathbf{Q}R$-shape. The transitions from convex to concave sections of the $\mathbf{Q}R$-shape correspond to the zero points of $\mathbf{S}R(\phi)$. The $\mathbf{Q}R$-shape yields the so-called dynamical Gibbs–Wulff shape, i.e. the crystal shape that develops from a point nucleus. In that case kinematic wave trajectories for the full orientation range $\phi = 0{-}2\pi$ emanate from this single point. The

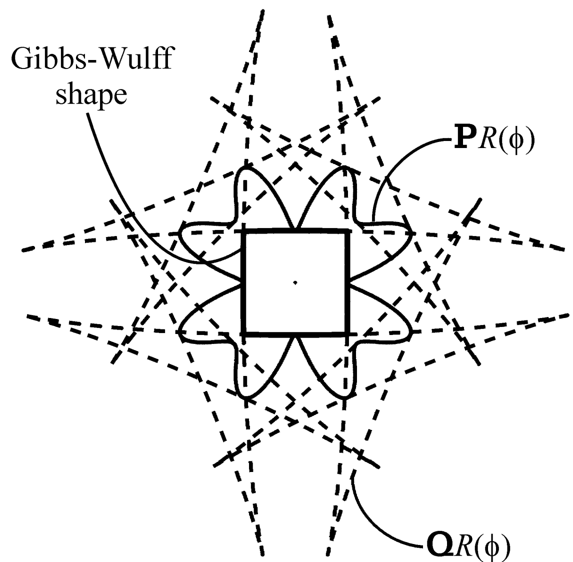

Fig. 1. The polar plot $\mathbf{P}R(\phi)$ for the advance rate, $R(\phi)$, used for all illustrations in Figs. 2–7. $R(\phi)$ is given by Eq. (4) with $v_{10} = v_{11}$ and $\varepsilon_{10} = 0.15$, $\varepsilon_{11} = 0.25$.

dynamical Gibbs–Wulff shape is obtained by removing the non-physical "ears" from the $\mathbf{Q}R$-shape, i.e. by only considering the inscribed figure.

It is instructive to compare the crystal shape evolution of an isolated protruding corner and an isolated re-entrant corner. In Fig. 2(a) the crystal surface evolving in a time t from a convex initial shape with a protruding corner is depicted. The crystal surface evolving from a concave initial shape with a re-entrant corner, complementary to the protruding corner in Fig. 2(a), is depicted in Fig. 2(b). Each point in a smooth section of the initial shape is displaced along its kinematic wave trajectory over the vector $t\mathbf{Q}R(\phi)$. In a corner of the initial shape kinematic wave trajectories emanate for all latently present orientations. Suppose that the normal orientations of the initial surface on both sides of the corner, with coordinate vector $\boldsymbol{s}$, are $\boldsymbol{n}_1$ and $\boldsymbol{n}_2$. Then the crystal surface at time t is completed by connecting the points $\boldsymbol{s} + t\mathbf{Q}R(\phi_1)$ and $\boldsymbol{s} + t\mathbf{Q}R(\phi_2)$ following the curve $\boldsymbol{s} + t\mathbf{Q}R(\phi)$ from ϕ_1 to ϕ_2. The "ears", cut short by the self-intersections, are non-physical and should be eliminated. For a protruding corner the relatively faster orientations are removed, while for a re-entrant corner the relatively slower orientations are removed. This implies that a crystal shape evolving from a protruding corner can only consist of convex sections of the $\mathbf{Q}R$ curve and that a crystal shape evolving from a re-entrant corner can only consist of concave sections. So we might say that a protruding corner is a "convex point source" and that a re-entrant corner is a "concave point source". A point nucleus is also an example of a convex point source, which explains that the dynamical Gibbs–Wulff shape only consists of convex sections.

3. The simulation algorithms

3.1. Representation of a surface

We assume that we have an analytical representation of the initial crystal shape. Of course, in order to calculate the evolution of this shape a discretization of the initial surface is required. We use a string representation for all surfaces, following the crystal interface in the direction that keeps the crystal on the left side of the interface. For each discretization point of the surface we store four data: the x- and y-coordinate and the normal orientations directly before and behind the point. Corners in the initial surface must be represented exactly. The orientations directly before and behind a discretization point are only different for corner points. The density of discretization points is determined by two resolutions: a resolution in the distance between points and a resolution in the difference in surface orientation between points. The angular resolution in particular determines the quality of the representation

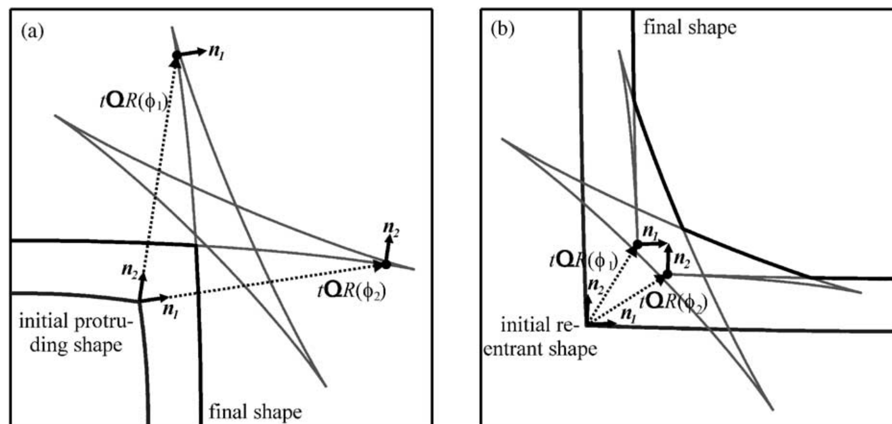

Fig. 2. Crystal shape evolution of an isolated protruding corner (a) and the complementary isolated re-entrant corner (b). (a) Slow orientations or convex sections in final shape, and (b) fast orientations or concave sections in final shape.

of the surface. The simulation algorithms described below maintain the angular resolution. The angular resolution of 1° used in this paper suffices to obtain smooth surfaces.

3.2. Convex or concave initial shapes

In this section we treat the evolution of crystals with an initial crystal shape that consists solely of convex or solely of concave sections. In this case, the final crystal shape can be calculated in a single time step for arbitrary evolution time t. All points on the discretized initial surface are displaced along their kinematic wave trajectories, over the vector $t\mathbf{Q}R(\phi)$. At a corner, with coordinate vector $\boldsymbol{s}$, extra points $\boldsymbol{s} + t\mathbf{Q}R(\phi)$ are added with the predefined angular resolution. These points correspond to kinematic wave trajectories for orientations that are latently present in the corner. Now, all we need to obtain the final crystal shape is an algorithm to cut off the unphysical ears. This algorithm we refer to as the vanGogh algorithm.

The concept that is the starting point of the vanGogh algorithm is illustrated in Fig. 3. In this figure an evolved shape is shown, corresponding to a convex initial shape, which contains an ear that is to be cut off to obtain the final shape. Now consider two points of the discretized initial surface A and B, for which the corresponding points on the evolved shape are on a concave part of this shape, which implies that the segment between A and B cannot be on the final shape. The kinematic wave trajectories of points A and B intersect. This is another condition that is sufficient to conclude that the segment between A and B will not be on the final shape. Hence, the first step of the vanGogh algorithm is determining for each segment of the evolved shape whether the kinematic wave trajectories corresponding to the start and end point of the segment intersect. The second step of the vanGogh algorithm is walking over the evolved surface segment-by-segment and checking for self-intersections of the current segment with segments that are already passed. Checking for self-intersections is only done if the presence of an unphysical ear is first detected, i.e. if first a section of the evolved surface is passed that cannot be on the final shape according to the first step of the algorithm. An adapted line-sweep algorithm is used to minimize the number of checks necessary to find possible self-intersections [13]. If a self-intersection is found, the corresponding ear is cut off the evolved surface. It is possible that after completing the walk over the surface one final ear must be cut off, because the starting segment is on this final ear.

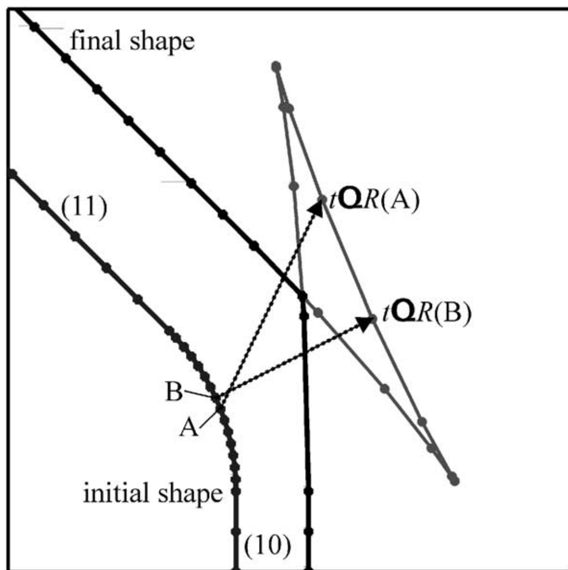

Fig. 3. The kinematic wave trajectories of point A and point B intersect, which implies that segment AB is not on the final shape.

In Fig. 4, several stages in the evolution of a dissolving crystal shape that consists completely of concave sections are drawn. Note that we call this crystal shape completely concave in accordance with the direction conventions of Section 2. The time interval between consecutive crystal shapes is constant. All crystal shapes are calculated in a single calculation step. The trajectories of the corner points are also indicated. These trajectories are only straight lines if the surface orientations on both sides of the corner are constant or if the symmetry of the crystal imposes this.

3.3. Mixed convex/concave initial shapes

In this section, we treat the evolution of crystals with an initial shape that consists of both convex

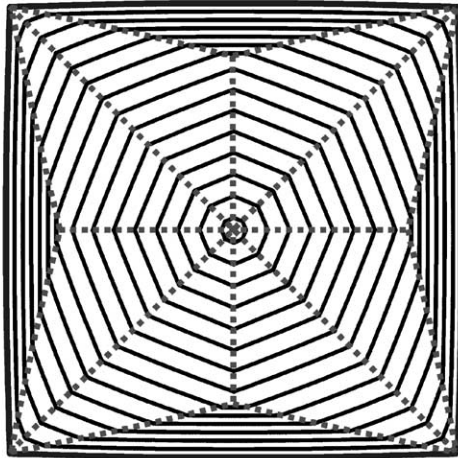

Fig. 4. Several stages in the evolution of a dissolving crystal shape that consists completely of concave sections. The trajectories of the corners are also depicted.

and concave sections. The calculation of the final crystal shape for a mixed convex/concave initial shape may require several time steps. The cause for this is the behavior of corners. In Section 2 a somewhat simplified picture of the evolution of a corner is presented. There it is stated that at $t = 0$ only, kinematic wave trajectories are emanating from the corner for all orientations latently present at the corner. In fact, new kinematic wave trajectories are emanating from the corner for all latently present orientations continuously. For a protruding corner, or convex point source, in a completely convex initial shape this amounts to the same. However, consider a protruding corner, or convex point source, bordered by a concave section of the surface. At such a corner certain orientations will vanish altogether from the crystal surface: relatively fast orientations present in the concave section drive out relatively slow orientations near the corner decreasing the range of orientations latently present in the corner. In a protruding corner only relatively slow orientations will develop, but it depends on the range of orientations latently present, which orientations are relatively slow. If this range becomes smaller, then new orientations may develop at the corner.

In most practical situations, the problem identified above will only have consequences when the trajectories of two corners, one stemming from a convex section or point source and another stemming from a concave section or point source, meet. An example of this behavior is presented in Fig. 5(a), which shows several stages in the evolution of a section of a crystal shape that contains a protruding and a re-entrant corner. In the initial crystal shape the protruding corner is bordered by two $\{1\,0\}$ surfaces. The evolving protruding corner initially remains bordered by vicinal $\{1\,0\}$ surfaces, see Fig. 2(a). In the re-entrant corner fast orientations develop, see Fig. 2(b). At some point in time t_c the protruding corner and a corner stemming from the re-entrant corner meet and merge into one corner. A whole range of orientations is annihilated at once. The result is a protruding corner bordered by one $\{1\,0\}$ surface and one fast surface in between $\{1\,0\}$ and $\{1\,1\}$. From this moment on a $\{1\,1\}$ surface develops at this corner, region A in Fig. 5(a). Note that the kinematic wave trajectories in this region all originate from the location of the protruding corner at $t = t_c$ and definitely not from the location of the protruding corner at $t = 0$. Therefore, the calculation of the evolution of this crystal shape for times $t > t_c$ can only be correct when using two time steps. First, using the simulation algorithm described in the previous section the crystal shape at time t_c should be calculated. A second calculation using the simulation algorithm, with the crystal shape at time t_c as initial shape, yields the desired final crystal shape.

Thus, every time when a corner stemming from a convex section of the surface merges with a corner stemming from a concave section of the surface, the calculation should be stopped and restarted. Unfortunately, there is, in our opinion, no general algorithm that can be used to identify the exact time t_c of occurrence of such an event. Hence, the user of the simulation tool will have to provide an upper bound of t_c. Usually, a small number of trial calculations are needed to determine such an estimate.

The vanGogh algorithm for cutting off unphysical ears from an evolved surface also becomes more complicated for mixed convex/concave initial shapes. Fig. 5(b) shows the evolved surface including unphysical ears corresponding to the time t_c that the protruding and re-entrant corner

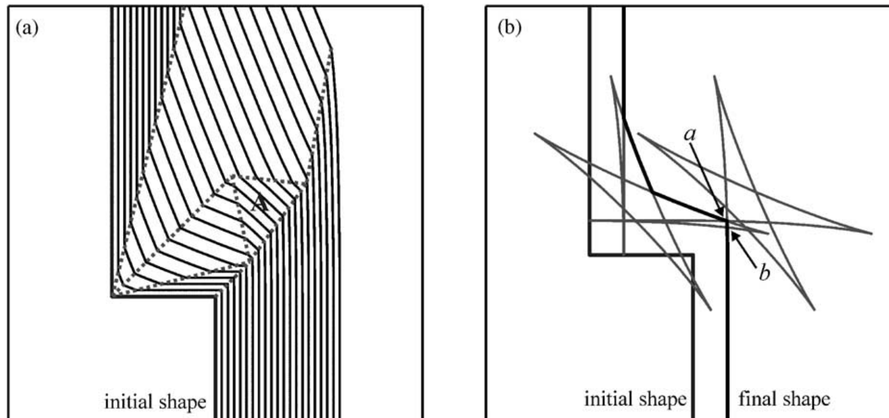

Fig. 5. (a) Several stages in the evolution of a section of a crystal shape that contains a protruding and a re-entrant corner. At time t_c the protruding and re-entrant corner meet and in the resulting protruding corner a {1 1} facet develops (region A). (b) The evolved surface including unphysical ears at time t_c.

meet, see also Fig. 5(a). At point *a* in the surface the two corners meet and two ears have to be cut off there. Two complications should be paid attention to. Observe that the ear corresponding to the re-entrant corner sticks outside the final shape at point *b*. This implies that in the second step of the vanGogh algorithm, segment-wise checking for self-intersections, the first found self-intersection after detecting this ear should be ignored. Here, the ear enters the crystal shape again; the second self-intersection that will be found shortly after the first should be used to cut off the unphysical ear. The second complication is even trickier. We need to be able to calculate reasonable crystal shapes for times t slightly larger than t_c, because we need to re-start the calculation just after the two corners merged into one. In the case of Fig. 5, this is only possible if after detecting that the ear corresponding to the re-entrant corner sticks out of the surface at point *b*, the ear already cut off at point *a* corresponding to the protruding corner is re-attached to the surface momentarily.

3.4. Velocity sources

The classical kinematic wave theory is limited to the evolution of isolated crystals, without complications due to grain boundaries, dislocations, stacking faults, foreign particles contaminating the surface, etc. Effectively this limitation implies that only the shape of a perfect single crystal, freely floating in a parent phase, is described correctly. In recent papers, we have treated the generalization of the kinematic wave theory to imperfect crystal surfaces [14,15]. There, we have coined the name velocity sources for those imperfections of the surface that locally change the advance rate and consequently the crystal shape. A point velocity source is completely defined by its velocity source vector $\mathcal{R}$. The direction of this vector is the direction in which the velocity source is advancing. The magnitude of this vector equals the advance rate imposed by the velocity source.

Consider the specific example of a velocity source accelerating growth on an initially flat {1 0} surface of our two-dimensional crystal, moving perpendicular to this surface. A stacking fault in a 2D crystal can act as velocity source of this type. In Fig. 6, this case is elaborated for two different magnitudes of the velocity source vector $\mathcal{R}$. To determine the effect of this velocity source on the evolution of the crystal surface, first the orientations $\boldsymbol{n}_1$ and $\boldsymbol{n}_2$ of the surfaces on both sides of the velocity source that remain connected to the source, which generate the so-called cone shape, need to be calculated. This is a simple calculation: the growth rate of these surfaces matches the advance rate of the velocity source and, therefore,

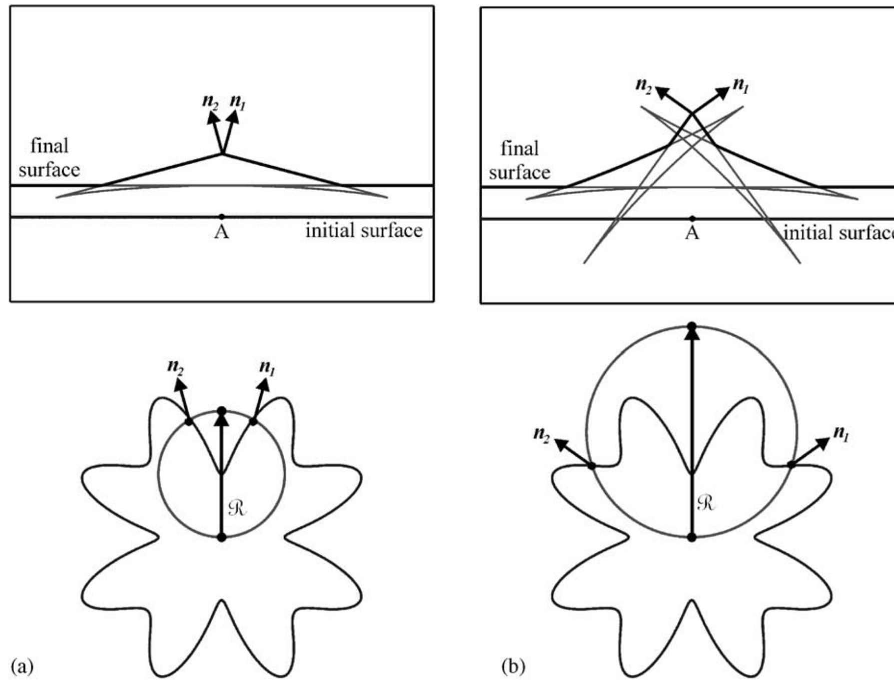

Fig. 6. Effect on the evolving crystal shape of a point velocity source accelerating growth on an initially flat {1 0} surface. The direction of the velocity vector $\mathcal{R}$ is perpendicular to the {1 0} surface. (a) Moderate value for the magnitude of the velocity vector $\mathcal{R}$. Evolving shape consists solely of the cone shape with orientations $\boldsymbol{n}_1$ and $\boldsymbol{n}_2$ cut off by the {1 0} surface. (b) Larger value for the magnitude of the velocity vector $\mathcal{R}$. In the re-entrant corners additional sections of fast orientations are formed.

the cone orientations can be found by calculating the intersections of the $\mathbf{P}R(\phi)$ plot and the circle through $\mathcal{R}$ and the origin, $\mathbf{P}[\mathcal{R}\boldsymbol{n}]$. The resulting cone orientations are shown in Fig. 6 for both choices of the magnitude of the velocity source vector.

The calculation of the evolution of the crystal surface is now straightforward. At $t = 0$ the velocity source is present as point A on the flat {1 0} surface. This single point has to be represented in the discretization of the surface by three points on this exact location: A_1, a re-entrant corner with orientations before and behind this point $\boldsymbol{n}_{\{10\}}$ and $\boldsymbol{n}_1$; A_2, the top of the cone shape; A_3, a re-entrant corner with orientations before and behind this point $\boldsymbol{n}_2$ and $\boldsymbol{n}_{\{10\}}$. The crystal shape can now be calculated as follows. Point A_2 has to be displaced over the distance $t\mathcal{R}$. The rest of the crystal shape can be calculated as before. Again, to obtain the final crystal shape we need to cut off the unphysical ears, using the vanGogh algorithm. Inspecting Fig. 6 it will be clear that it depends on the magnitude of the velocity source vector whether the hillock, which arises around the velocity source, consists solely of the cone shape. In Fig. 6(b) an additional section of fast orientations develops in the re-entrant corners of the cone shape.

3.5. Interacting initial shapes

The simulation tool includes an algorithm that deals with the possibility of two or more disconnected crystal shapes meeting at some point in their evolution. A prerequisite of this algorithm is that the overall crystal orientation of two meeting crystal shapes is identical. This seems a severe restriction, but the algorithm actually has some important applications. One application is the evolution of step patterns. Step contours auto-

matically have the same orientation, as the underlying crystal lattice acts as a template [16]. Another application is presented in the next section: etching of a masked single crystal wafer with multiple mask openings.

If two crystal shapes meet in the course of their evolution, it is necessary to calculate the exact time t_m that the two crystal shapes touch. At that exact moment, two surfaces merge into one and quite likely two re-entrant corners are formed at the meeting point. Therefore, the calculation must be stopped and re-started at time t_m: new fast orientations will develop in the re-entrant corners. An example of this behavior is given in Fig. 7(a), which shows two meeting convex crystal shapes evolving from two identical circular initial shapes. Note that when two convex crystal shapes meet, the combined crystal shape is mixed convex/concave, which means that further calculation of the crystal shape evolution requires extra caution.

The algorithm used to automatically find the time t_m that two crystal shapes meet is based on iteration. The first iteration step starts by calculating the two final crystal shapes corresponding to an evolution time $t_1 > t_m$, where t_1 equals the final time t. These two curves have one or more pairs of intersections, which are found using an adapted line sweep algorithm [13]. For instance, in the case of Fig. 7 one pair of intersections, A and B, is found, see Fig. 7(b). Subsequently, for a pair of intersections it is determined which segments on both curves are (partly) inside the other curve. For each kinematic wave trajectory corresponding to the start or end point of one of these segments, which ends inside the other curve, the reduced evolution time that makes that this trajectory would no longer end inside but end exactly on the other curve is calculated. The minimum of these reduced evolution times is still an upper bound of the meeting time t_m, and this time is used as time t_2 in the second iteration step. The second iteration step starts by calculating the two final crystal shapes corresponding to an evolution time $t_2 > t_m$. The iteration stops when the reduction in time $t_{i+1} - t_i$ becomes lower than a preset threshold. Then the meeting time is identified with t_{i+1}, i.e. $t_m = t_{i+1}$, and the two crystal shapes are merged into one.

For some initial crystal shapes it might occur that one part of an evolving crystal shape touches another part of this same crystal shape at some point in time. In general, the simulation tool cannot handle such an event.

4. Wet chemical etching of silicon

Anisotropic wet chemical etching of masked {1 0 0} single crystal silicon wafers is used for fast and reproducible shaping of micromechanical

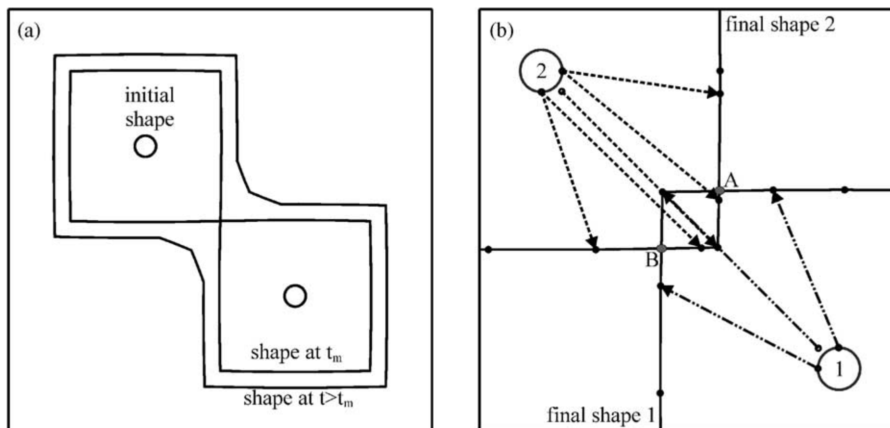

Fig. 7. (a) Two convex crystal shapes, meeting at time t_m, evolving from two identical circular initial shapes. (b) Illustration of the algorithm for finding time t_m; all relevant (virtual) kinematic wave trajectories are shown.

structures in the fabrication of microsystems [17]. Nowadays the anisotropic etching technology is used in the fabrication of devices that range from pressure sensors and accelerometers to sensors for flow, temperature, force, position, magnetic fields, chemicals, light, etc. Frequently, the complexity of the desired microstructure demands an anisotropic etching step that involves multiple mask openings on both sides of a silicon wafer. In this section, a simple example of such an etching experiment is compared with a simulation.

4.1. Description of the experiment

In the experiment a Si{1 0 0} wafer is etched from both sides in a strongly alkaline KOH water solution (25 wt% KOH) at a temperature of 70°C. A cross-section of the wafer through [1 0 0] and [0 1 1] is depicted in Fig. 8(a). The thickness of the wafer is approximately 380 μm and the silicon nitride masks on both sides are applied on a lateral distance of 260 μm. The mask edges are aligned along [0 1 $\bar{1}$].

Necessary for performing a simulation is detailed knowledge of the etch rate of silicon in KOH for the chosen experimental conditions in the crystallographic zone through [1 0 0] and [0 1 1]. Fortunately, the complete orientation dependence of the etch rate of silicon in 26 wt% KOH at 70°C has been measured comprehensively by Sato et al. [18], using a sphere etch experiment. In previous work, we have formulated an analytical etch rate function containing only nine parameters, which is shown to describe this experimental etch rate very well [9]. In Fig. 8(b) the experimental and the analytical etch rate in the zone through [1 0 0] and [0 1 1] are both depicted. Clearly, the analytical etch rate function is a good representation of the experimental etch rate.

The etch rate of a {1 1 1} surface is very low; the exact value of this etch rate cannot be obtained in a sphere etch experiment. Therefore, we have used a value obtained in an underetch experiment [19], $R(1\,1\,1) = 15.8$ nm/s. A complication of the experiment is that the junction between a silicon nitride mask and a Si{1 1 1} surface can act as a velocity source. Experimentally, it is found that a Si{1 1 1} surface with an obtuse contact angle with the mask of approximately 125° etches faster than a Si{1 1 1} surface with an acute contact angle with the mask of approximately 55° [19,20]. For an acute contact angle the mask junction does not act as a velocity source. The reason for the velocity source behavior for a large contact angle is that beyond a certain value for the contact angle, 1D nucleation of steps at the mask is faster than the nucleation processes

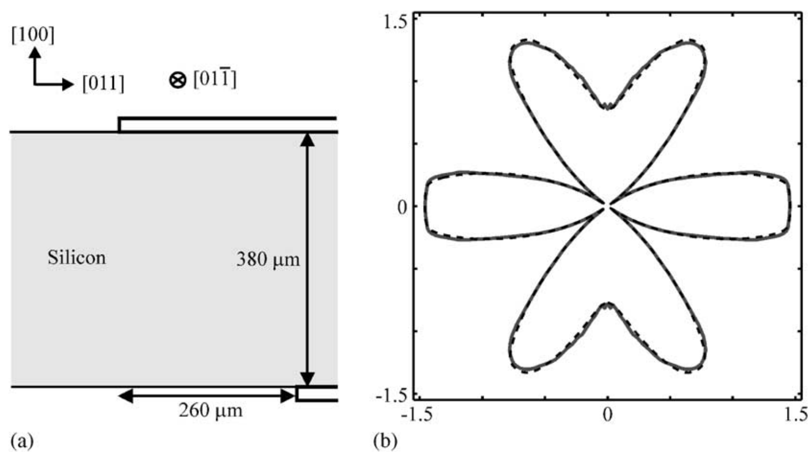

Fig. 8. (a) Cross-section of the Si{1 0 0} wafer used in the etching experiment. On both sides of the wafer a mask is present. The mask edges are aligned along [0 1 $\bar{1}$]. (b) Polar plot of the etch rate of silicon in 26 wt% KOH at 70°C in the crystallographic zone through [1 0 0] and [0 1 1]. The solid line corresponds to the measurement of Sato et al., while the dashed line represents the analytical expression for the etch rate used in the simulation.

on the {1 1 1} surface [19,21]. Specifying the velocity source vector $\mathscr{R}_{111}$ for this case is very simple: the direction of the vector is the direction along the mask into the silicon crystal, and the magnitude of the vector is the measured underetch rate of a Si{1 1 1} surface with an obtuse contact angle [19], $|\mathscr{R}_{111}| = 29.4$ nm/s.

4.2. Simulation

The simulation of the etching experiment uses all the simulation algorithms presented in Section 3. In Fig. 9(a) 27 consecutive stages of etching with a time interval of 25 min are shown.

There are two initial shapes: on the upside of the wafer a (1 0 0) oriented surface starting at a mask junction and on the downside of the wafer a ($\bar{1}$ 0 0) oriented surface ending at a mask junction. The corners at the mask are disguised protruding corners. The orientations directly before and after the corner for both the mask corner on the upside and the mask corner on the downside of the wafer correspond to [$\bar{1}$ 0 0] and [1 0 0], respectively. The difference in orientation is as large as 180° in order to allow all possible contact angles of the silicon surface with the mask. For each time step, the final shape is calculated using the algorithms explained in Section 3. After this calculation an additional step is necessary. The mask acts as a boundary of the validity range of the solution; the parts of the final shape beyond the mask boundary have to be cut off. If more than one time step is necessary, then the orientation directly before the top mask corner should be reset to [$\bar{1}$ 0 0] and the orientation directly behind the bottom mask corner should be reset to [1 0 0].

The initial shapes are completely convex. In the initial stages two trenches are formed, bounded by Si{1 1 1} surfaces with an acute contact angle with the mask and by {1 0 0} bottom surfaces. After 245.5 min of etching, these two trenches meet each other. From that moment, only one crystal shape remains, which connects the upside mask with the downside mask, and which consists of both convex and concave sections: a re-entrant corner is formed the moment the wafer is etched through. From this re-entrant corner two sets of fast orientations emerge: the re-entrant corner splits up into three

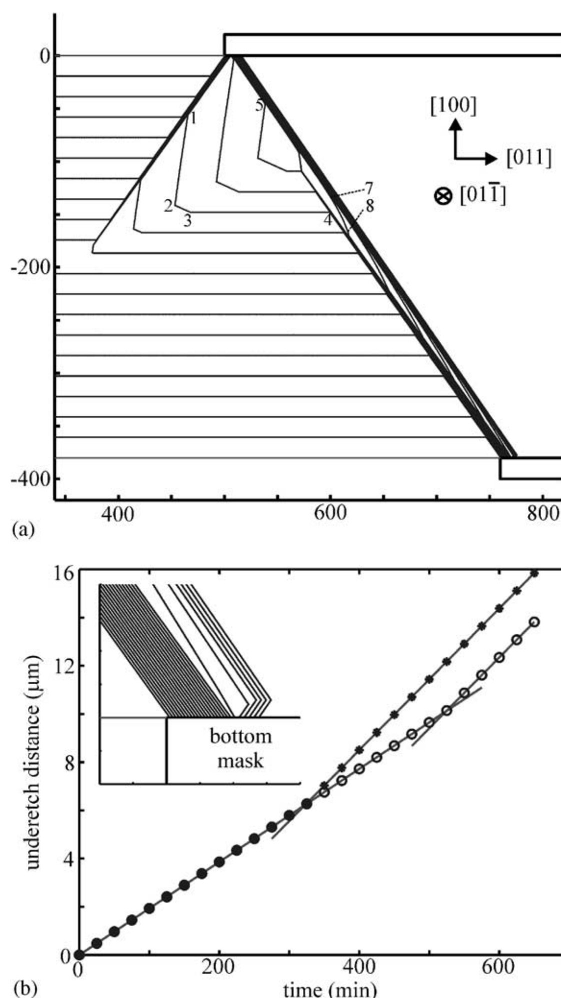

Fig. 9. (a) Simulation of the etching experiment. Twenty-seven consecutive stages of etching with a time interval of 25 min are shown. The numbers depicted at corners in some of the stages correspond to the numbering used in the text. Re-entrant corner 6 is not resolved in this series of stages. (b) The underetch distance as a function of time for both the upside (stars) and the downside (circles) of the wafer. The inset shows the detailed evolution of the crystal shape at the mask junction on the downside of the wafer.

re-entrant corners. From the upside mask to the downside mask, the crystal shape now consists of a {1 1 1} surface (acute contact angle), a vicinal {1 1 0} surface, a fast orientation in between {1 1 1} and {1 0 0}, a {1 0 0} surface and again a {1 1 1} surface (acute contact angle). From the upside mask to the downside mask, we encounter the

protruding upside mask corner, re-entrant corner 1, re-entrant corner 2, re-entrant corner 3, protruding corner 4 and the protruding downside mask corner.

After 323 min of etching, the trajectory of the re-entrant corner 1 meets the trajectory along the mask of the protruding upside mask corner. This means that the calculation must be stopped and re-started. From this moment on, a Si{1 1 1} surface with an obtuse contact angle will develop. The upside mask corner is a velocity source that propagates with vector velocity $\mathcal{R}_{111}$. Besides the protruding mask corner a new protruding corner 5 is formed, connecting the {1 1 1} surface (obtuse contact angle) and the vicinal {1 1 0} surface. Further in the evolution of the surface the calculation needs to be stopped five more times. The first time (356 min) is when the trajectory of the re-entrant corner 3 meets the trajectory of the protruding corner 4. No new orientations are formed; protruding corner 4 now connects the fast orientation in between {1 1 1} and {1 0 0} and the Si{1 1 1} surface (acute contact angle). The second time (364.5 min) is when the trajectories of re-entrant corner 2 and protruding corner 4 meet; re-entrant corner 2 persists and now connects the vicinal {1 1 0} surface and the Si{1 1 1} surface (acute contact angle). After a short time of etching a new re-entrant corner 6 is formed connecting the vicinal {1 1 0} surface and a second vicinal {1 1 0} surface slanted in the other direction with respect to (0 1 1). The third time that the calculation must be stopped and re-started (372 min) is when the trajectories of protruding corner 5 and re-entrant corner 6 meet. The newly formed protruding corner splits up in two protruding corners 7 and 8. The fourth time (404 min) is when the trajectories of protruding corner 8 and re-entrant corner 2 meet; re-entrant corner 2 persists. The fifth time (524.5 min) is when the trajectories of re-entrant corner 2 and the protruding downside mask corner meet. From this moment on, also on the downside of the wafer a Si{1 1 1} surface with an obtuse contact angle will develop. Again, the downside mask corner is then a velocity source that propagates with vector velocity $\mathcal{R}_{111}$. The evolution of the crystal shape at the mask junction on the downside of the wafer is shown as an inset of Fig. 9(b). Fig. 9(b) shows a graph of the underetch distance as a function of time for both the upside and the downside of the wafer. The graph clearly shows the very fast flipping from a Si{1 1 1} surface with acute contact angle to a Si{1 1 1} surface with obtuse contact angle after 323 and 524.5 min, respectively [19].

4.3. Comparison simulation and experiment

Two Si{1 0 0} wafers are etched in 25 wt% KOH at 70°C, one for a total etching time of 300 min and one for 397 min. On the wafers silicon nitride mask patterns are applied such that the cross-sectional configuration of Fig. 8(a) occurs several times on the wafer. After etching, the etched structures are embedded in epoxy resin in order to facilitate sawing the desired cross-sections. Cross-sections on the same wafer, i.e. etched for the same etching time, are perfectly identical. In Figs. 10(a) and 10(c) the resulting experimental cross-sections are given.

In Fig. 10(b) the simulated and the experimental cross-sectional crystal shape corresponding to an etching time of 300 min are compared. It is obvious that the absolute scaling of the etch rate (Fig. 8(b)) is not correct. The experimental crystal shape after 300 min has evolved further than the simulated crystal shape. The experimental etch rate of {1 0 0}, and we assume the etch rate for any other orientation, is about 15 percent higher than the analytical etch rate depicted in Fig. 8(b). Apart from the time scaling, both cross-sections are very similar. The same fast orientations in between {1 1 1} and {1 0 0} have emerged from the re-entrant corner formed when etching through the wafer. Also, in both cases a vicinal {1 1 0} surface is formed with virtually the same misorientation with respect to (0 1 1). A very important difference, however, is that in the experimental cross-section the vicinal {1 1 0} surface is slanted in the opposite direction.

In Fig. 10(d), the simulated and the experimental cross-sectional crystal shape corresponding to an etching time of 397 min are compared. Remarkably, in this case, the experimental and the simulated cross-section seem to be in almost the same stage of their evolution. We feel this is a

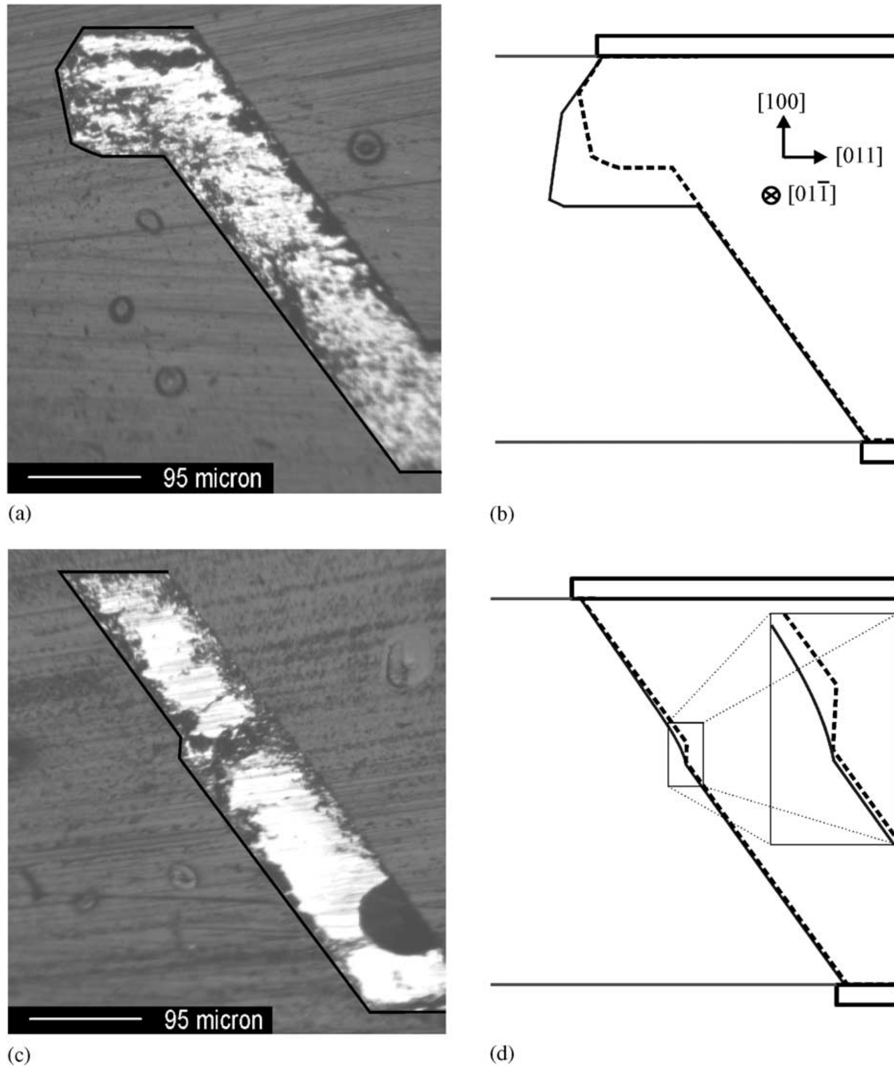

Fig. 10. Comparison of the etching experiment and the simulation. (a) Experimental cross-section after 300 min of etching, (b) simulated (solid line) and experimental (dashed line) cross-section at $t = 300$ min, (c) experimental cross-section after 397 min of etching and (d) simulated (solid line) and experimental (dashed line) cross-section at $t = 397$ min.

coincidence: two opposite effects canceling each other. There are two important differences. Firstly, the vicinal Si{1 1 0} surface in between the two Si{1 1 1} surfaces found in the experimental cross-section is again slanted in the opposite direction as the Si{1 1 0} surface in the simulation. Secondly, in the simulation slow orientations are emerging in the protruding corner between the Si{1 1 1} surface (obtuse contact angle) and the vicinal Si{1 1 0} surface. This is a direct consequence of the first difference. Protruding corner 5 in the simulation connects a {1 1 1} surface (obtuse contact angle) and a vicinal {1 1 0} surface slanted in the same direction as the surface in the experimental cross-section in Fig. 10(c). In this corner, no slow orientations emerge. Only after protruding corner 5 and re-entrant corner 6 meet and an oppositely slanted Si{1 1 0} surface is connected with the

Si{1 1 1} surface, in the simulation slow orientations emerge in the protruding corner. On the other hand, it would seem that in the experiment fast orientations should emerge in the re-entrant corner between the vicinal Si{1 1 0} surface and the Si{1 1 1} surface (acute contact angle), which obviously is not the case.

In order to find an explanation for the differences, we need to consider the mesoscopic details of the etching mechanism of Si{1 1 0} surfaces. For silicon etched in KOH with a concentration lower than approximately 40 wt%, exact Si{1 1 0} surfaces break up in a staircase or zig-zag pattern [9,22–24]. The zig and zag surfaces are inclined towards the adjacent {1 1 1} surfaces. For vicinal Si(1 1 0) surfaces inclined towards {1 1 1} the surface is still dominated by an asymmetric zig-zag pattern up to the inclination of the zig and zag surfaces. The re-entrant edges are velocity sources, moving perpendicular to the {1 1 0} surface. In the orientation range between the zig and the zag orientation the etch rate equals the velocity source rate, as can be seen in Fig. 8(b). We have hypothesized that this velocity source behavior can be explained by the presence of silicate particles adhering to the surface [24]. Tiny silicate particles are formed continuously during etching and are deposited uniformly on the surface. Some are somewhat larger than others and, consequently, slow down etching locally, initiating the formation of a re-entrant edge. Once an initial edge is formed, this edge starts to act as a sink of silicate particles. Most of the silicate particles present on the surface do not seriously affect the etch rate, but they keep attached to the surface and, as a consequence, follow trajectories that are on average perpendicular to the local surface. As a result, for a zig-zag surface, these particles assemble on the re-entrant edges.

We feel that the differences between the experiment and the simulation might be explained by realizing the following. Using the etch rate of Fig. 8(b) in the simulation, essentially means that we assume that a zig-zag pattern is immediately formed on an emerging Si{1 1 0} surface. Sato et al. have shown that in reality it takes time before a zig-zag pattern is formed [22]. Thus, a Si{1 1 0} surface emerging from a corner is initially flat, before a zig-zag pattern is formed. Apparently, the dependence of the etch rate of such a developing surface on the time elapsed, i.e. on the stage of development of the zig-zag surface, is quite complex. Very small local variations in the etch rate of short duration may very well explain the etching behavior found experimentally in Fig. 10. If this is true, then it is impossible to reproduce the experiment using any simulation tool based on the kinematic wave theory, i.e. on the assumption that the etch rate depends solely on the surface orientation. Any successful simulation would have to incorporate a detailed account of the formation of the zig-zag pattern on all emerging Si{1 1 0} surfaces.

5. Extension to three dimensions

Extension of the simulation algorithms from two to three dimensions is not straightforward at all. Already the representation of three-dimensional surfaces presents difficulties. Discretizing an arbitrary initial surface is not a simple task in itself, but especially it will be difficult to find a general recipe to describe the orientations that are latently present in a vertex of a three-dimensional crystal shape.

For a completely convex or a completely concave initial three-dimensional crystal shape it is easy to visualize the evolution in time of the crystal shape based on the simulation algorithms presented in Section 3.2. Again a single calculation step suffices. It is straightforward to find the evolved shape including unphysical ears. However, removing three- instead of two-dimensional ears is much more complicated. Extension of the vanGogh algorithm is not possible for two reasons. Firstly, there is no natural ordering of discretization points on the surface, which is essential in both steps of the vanGogh algorithm. Secondly, the detection of an unphysical ear using the principle of intersecting kinematic wave trajectories (see Fig. 3) does not work in three dimensions. In three dimensions it is very likely to find that the kinematic wave trajectories of two neighboring discretization points cross instead of intersect. Hence, a different algorithm has to be

developed to cut off unphysical ears in three dimensions.

The most important hurdle, however, is the extension to three dimensions of the calculation of the evolution of mixed convex/concave initial crystal shapes. In Section 3.3, we have found that in two dimensions the presence of both convex and concave sections in the initial crystal shape complicates the algorithm for cutting off ears considerably, and that more than one calculation step may be required to obtain the final crystal shape. In three dimensions the necessary adjustments to the algorithm for cutting off ears are even more challenging. The detection of points in time where the interaction of convex and concave sections requires stopping and re-starting the calculation algorithm is another extremely difficult task. It should be realized also that, in certain cases, the calculation algorithm should be stopped immediately at $t = 0$. The reason for this is that in a three-dimensional surface not only protruding and re-entrant vertices but also saddle-type vertices can occur. A saddle-type vertex has a mixed convex/concave character. A moving vertex adds length to at least one of the edges connected to the vertex. This means that the new kinematic wave trajectories that are continuously emitted by the vertex may affect the evolving shape. For re-entrant and protruding vertices it can be shown that this does not change the evolving shape. In the case of a saddle-type vertex it may lead to the nucleation of new conical surfaces. As a result other saddle-type corners may be generated immediately at $t = 0$. In turn, these generated saddle-type corners may nucleate another set of new conical surfaces, etc. The evolution of saddle-type corners is the subject of another, dedicated paper [25,26].

In conclusion, for simulation of three-dimensional crystal shape evolution it is probably best to develop a simulation algorithm that proceeds in small time steps. Still, it would be necessary to develop algorithms to calculate the evolution at edges (protruding and re-entrant) and at corners (protruding, re-entrant and all different saddle-types [25,26]). Additionally, another algorithm should be devised that decides when edges/corners that are very close to each other should be combined into one edge/corner. Of course, the numerical precision of such a simulation tool is probably not optimal; all rounding and discretization errors will be amplified due to the explicit simulation algorithm used.

6. Conclusion

A simulation tool for crystal shape evolution in two dimensions is presented for the case that the advance rate of the surface solely depends on the surface orientation. The number of time steps necessary to calculate the final crystal shape at some time t is one for completely convex or completely concave initial crystal shapes and a small number for mixed convex/concave initial crystal shapes, depending on the complexity. Accordingly, the calculated final crystal shape is very close to the mathematically exact final crystal shape. The simulation tool can cope with boundary conditions imposed at imperfections or other boundaries acting as velocity sources. The tool can also deal with multiple crystal shapes that merge at some point in their evolution.

We have applied the simulation tool to the technologically relevant case of wet chemical etching of masked silicon $\{1\,0\,0\}$ wafers with multiple mask openings. This example uses all the features of the simulation tool. Also, the example clearly shows a limitation of this type of continuum simulations. If in an experiment the advance rate locally deviates from the advance rate used in the simulation, even if it is only for a short duration, this may induce essential differences between experiment and simulation.

Extension of our simulation algorithms to three dimensions is extremely challenging. It seems most promising to develop a simulation tool that is based on an explicit calculation scheme of small time steps.

Acknowledgements

It is a pleasure for the authors to acknowledge Prof. K. Sato (Nagoya University, Japan), who has supplied the experimental silicon etch rate used

in Section 4. We would also like to thank P. Leusink for valuable discussions on the interpretation of the silicon etching experiments in Section 4. This work is supported by the Dutch Technology Foundation (STW).

References

[1] W.K. Burton, N. Cabrera, F.C. Frank, Phil. Trans. Roy. Soc. London A 243 (1951) 299.
[2] P. Bennema, J.P. van der Eerden, in: I. Sunagawa (Ed.), Morphology of Crystals Part A, Terrapub, Tokyo, 1987, p. 1.
[3] J.P. van der Eerden, in: D.T.J. Hurle (Ed.), Handbook of Crystal Growth, Vol. I, Elsevier, Amsterdam, 1993, p. 307.
[4] W.W. Mullins, R.F. Sekerka, J. Appl. Phys. 34 (1963) 323.W.W. Mullins, R.F. Sekerka, J. Appl. Phys. 35 (1964) 444.
[5] J.E. Taylor, J.W. Cahn, C.A. Handwerker, Acta Metall. Mater. 40 (1992) 1443.
[6] F.C. Frank, in: R.H. Doremus, et al., (Eds.), Growth and Perfection of Crystals, Wiley, New York, 1958, p. 411.
[7] A.A. Chernov, Sov. Phys. Crystallogr. 8 (1963) 401.
[8] J. van Suchtelen, E. van Veenendaal, J. Appl. Phys. 87 (2000) 8721.
[9] E. van Veenendaal, J. van Suchtelen, W.J.P. van Enckevort, K. Sato, A.J. Nijdam, J.G.E. Gardeniers, M. Elwenspoek, J. Appl. Phys. 87 (2000) 8732.
[10] I.V. Katardjiev, G. Carter, M.J. Nobes, J. Phys. D: Appl. Phys. 22 (1989) 1813.
[11] J. van Suchtelen, in: I. Sunagawa (Ed.), Morphology of Crystals C, Terrapub, Tokyo, 1995.
[12] J.W. Cahn, W.C. Carter, Metall. Mater. Trans. 27A (1996) 1431.
[13] M. de Berg, M. van Kreveld, M. Overmars, O. Schwarzkopf, Computational Geometry: Algorithms and Applications, Springer, Berlin, 1997.
[14] J. van Suchtelen, A.J. Nijdam, J.G.E. Gardeniers, M. Elwenspoek, E. van Veenendaal, W.J.P. van Enckevort, E. Vlieg, Phys. Rev. B. (2000), submitted for publication.
[15] J. van Suchtelen, A.J. Nijdam, E. van Veenendaal, J. Crystal Growth 198–199 (1999) 17.
[16] E. van Veenendaal, F.K. de Theije, J. van Suchtelen, W.J.P. van Enckevort, Diamond Related Mater. (2000), in press.
[17] M. Elwenspoek, H.V. Jansen, (Eds.), Silicon Micromachining, Cambridge University Press, Cambridge, 1998.
[18] K. Sato, M. Shikida, Y. Matsushima, T. Yamashiro, K. Asaumi, Y. Iriye, M. Yamamoto, Sensors Actuators A 64 (1998) 87.
[19] A.J. Nijdam, J.G.E. Gardeniers, J.W. Berenschot, E. van Veenendaal, J. van Suchtelen, M. Elwenspoek, J. Micromech. Microeng. 11 (2001) 499.
[20] A.J. Nijdam, J. van Suchtelen, J.W. Berenschot, J.G.E. Gardeniers, M. Elwenspoek, J. Crystal Growth 198/199 (1999) 430.
[21] E. van Veenendaal, H.M. Cuppen, W.J.P. van Enckevort, J. van Suchtelen, A.J. Nijdam, M. Elwenspoek, E. Vlieg, J. Micromech. Microeng. 11 (2001) 409.
[22] K. Sato, M. Shikida, T. Yamashiro, M. Tsunekawa, S. Ito, Sensors Actuators A 73 (1999) 122.
[23] E. van Veenendaal, K. Sato, M. Shikida, J. van Suchtelen, Sensors Actuators A 93 (2001) 219.
[24] E. van Veenendaal, K. Sato, M. Shikida, A.J. Nijdam, J. van Suchtelen, Sensors Actuators A 93 (2001) 232.
[25] J. van Suchtelen,E. van Veenendaal, Phys. Rev. B (2001), submitted for publication.
[26] J. van Suchtelen, E. van Veenendaal, Sensors and Materials 13 (2001) 325.